THE JOURNAL OF PHYSICAL CHEMISTRY C
A JOURNAL OF THE AMERICAN CHEMICAL SOCIETY

pubs.acs.org/JPCC

Article

Thickness Fluctuations Produce Apparent Long-Range Tunneling in Large-Area Junctions: The Case of Polyelectrolyte Multilayers

Liliana Maldonado, Santiago E. Herrera,* Federico J. Williams, and Mario Tagliazucchi*

Cite This: J. Phys. Chem. C 2022, 126, 9956−9964

Read Online

ACCESS | Metrics & More | Article Recommendations | Supporting Information

ABSTRACT: The electron-tunneling (ET) current through a barrier of thickness h is generally analyzed with the Simmons model, $j \sim \exp(-\beta h)$, where β is the tunneling decay coefficient. We show that fluctuations in barrier thickness produce apparent β values systematically smaller than the real ones, which may lead to incorrectly postulating long-range electron tunneling. We reached this conclusion by performing the first tunneling studies through polyelectrolyte-multilayer films of different average thicknesses using impedance spectroscopy and EGaIn/Ga_2O_3 top contacts. We explained these measurements with a model that considers ET through a film with a Gaussian distribution of thicknesses, as observed by atomic force microscopy. It is shown that even relatively small thickness fluctuations can introduce a systematic error in the determination of β and that when the average film thickness and its standard deviation become commensurable, it is impossible to determine β.

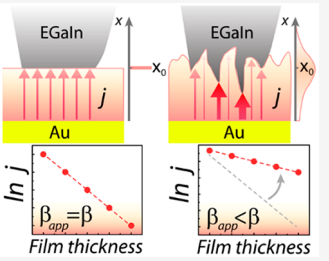

INTRODUCTION

Electron tunneling through large-area soft-matter junctions is a process of practical importance for the development of molecular electronics. Tunneling currents are measured between the conducting substrate where the organic film is deposited and a top contact made of evaporated gold,[1] graphene,[2] Hg,[3,4] conductive polymers,[5] an AFM/STM tip[6,7] or EGaIn/Ga_2O_3[8−12] using either direct current (DC)[12] or alternating current (AC)[9] methods. The most commonly studied junctions are those of self-assembled monolayers (SAMs)[8,13] because of their high degree of molecular order and the control over film thickness exerted by the molecular length. In addition to SAMs, tunneling through (less ordered) protein films has also been studied.[14,15] The tunneling current (j) is generally analyzed in terms of the simplified Simmons model in the low-bias regime ($eV \sim 0$):[16,17]

$$j(V) = j_0(V)\exp(-\beta h) \quad (1)$$

where h is the thickness of the insulating film, β is the tunneling decay constant, and j_0 is the injection tunnel current density (ideal current for $h = 0$). Here, $\beta = 2\left(\frac{2m\tilde{\varphi}}{\hbar^2}\right)^{1/2}$, with m the mass of the electron and $\tilde{\varphi}$ the mean barrier height energy between the Fermi level of the electrode and the molecular frontier orbital. Also, according to the Simmons model in the low-bias regime, j_0 must follow a linear dependence on the applied potential (ohmic response).

A major impediment for the advancement of the field is the dispersion in the values of the tunneling parameters, β and j_0, measured for SAMs.[4,11,18] Alkanethiol SAMs are perhaps the system where off-resonance electron tunneling was studied in most detail because of their well-known compact packing over Au surfaces. In the case of Au−SH−$(CH_2)_n$−SH−Au molecular junctions, it was demonstrated that the β value for electron tunneling is around 1 per methylene (CH_2) unit[19,20] ($\beta \sim 0.8$ Å^{-1}). However, it was also shown that this value decreases when the thiol anchoring groups are replaced by $-NH_2$ ($\beta_{NH_2} \sim 0.9/CH_2$),[21] −COOH ($\beta_{COOH} \sim 0.8/CH_2$),[22,23] and highly polarizable atoms like iodine ($\beta_I \sim 0.5/CH_2$).[24] Moreover, Chen et al. showed that by varying X = H, F, Cl, Br, I in small area EGaIn junctions (350 μm^2) with $S(CH_2)_{(10-18)}X$, molecular conductors showed a reduction of β from 0.75 to 0.25 Å^{-1}.[25] These effects arise because of subtle alterations in the HOMO−LUMO gaps, localized potential drops, and dielectric constants, which have an impact on tunneling barrier heights and even in the tunneling mechanism itself. On the other hand, molecules that contain a conjugated moiety (phenyl, viologen, or α-terthiophene) in the center of alkane chains of varying length gave rise to resonances close to the Fermi level through coupling to the bridge moiety. In those cases, β values ranging from 0.9 Å^{-1} (alkanedithiol) to 0.07 Å^{-1} (alkanedithiol with a α-terthiophene central unit)[26] were measured. Lastly, long-range electron conductance was observed for more complex systems as in the case of proteins,[14,27] although the mechanism of conduction is not definitively established.[28,29]

Received: March 30, 2022
Revised: May 19, 2022
Published: June 2, 2022

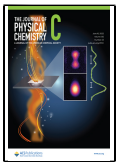

https://doi.org/10.1021/acs.jpcc.2c02175
J. Phys. Chem. C 2022, 126, 9956−9964

The roughness, molecular organization, and presence of defects in the barrier and/or the substrate can influence the determination of β in large-area junctions. Nijhuis and co-workers reported β values 60% smaller than the expected ones for alkanethiol SAMs on rough substrates.[18] The authors ascribed this effect to the deformation of the thiol layer at the grain boundaries of the rough surface.[18] Other works reported β values for SAMs outside the consensus range (0.73−0.89 $Å^{-1}$ [11]) and ascribed them to factors such as defects or pinholes,[4,30,31] the effect of the electric field on molecular conformations,[32] changes in the tunneling pathway or mechanism,[3,7,14,17] and the physical deformation of the film under applied mechanical loading.[6] None of these mechanisms were supported by a quantitative model capable of predicting the tunneling parameters. Moreover, information on which variables affect the determination of the tunneling parameters in ultrathin films different from SAMs is extremely scarce. There is, therefore, a need to develop quantitative and generally applicable insights of how and why variables such as the roughness, presence of defects, and molecular organization of soft-matter large-area junctions influence the determination of the tunneling parameters.

This work reports the first measurements of electron tunneling through ultrathin polyelectrolyte multilayers.[33,34] We analyze these experimental results with a theoretical model for electron tunneling through an inhomogeneous film. This analysis demonstrates that the intrinsic thickness fluctuations of polyelectrolyte multilayers produce very low apparent tunneling decay coefficients, which may incorrectly lead one to postulate the existence of long-range electron tunneling. It is important to note that "thickness fluctuations" are not equivalent to surface roughness (a factor that was previously proposed to yield smaller-than-expected β values[18]). For example, thiol SAMs may be rough because of the roughness of the underlying substrate, even if their thickness is very homogeneous.

MATERIALS AND METHODS

Materials. Poly(acrylic acid) sodium salt, PAA (35% in water Mw 100 000); poly(allylamine) hydrochloride, PAH (Mw 58 000); and sodium 3-mercapto-1-propanesulfonate, MPS, were obtained from Sigma-Aldrich. Polyelectrolyte solutions were prepared with 18 MΩ Milli-Q (Millipore) deionized water, and their pH was adjusted using 1 M HCl or NaOH solutions. Eutectic metal alloy EGaIn (75.5% Ga and 24.5% In by weight) was prepared by dissolving 3.384 g of In wire (99.995%, Sigma-Aldrich) in 10.429 g of Ga 99.99% (Rotometals, CA, USA) in a hot (∼70 °C) water bath. Other reagents were analytical grade, and they were used without further purification.

Preparation of Template-Stripped Gold Substrates. Template-stripped (TS) gold substrates were prepared following the method of Weiss et al.[35] A Si/SiO_2 (100) wafer was first coated with a 200 nm gold layer by thermal evaporation in an Edwards Auto 306 vacuum coating system at a pressure of $<1.10^{-8}$ bar. A drop of Norland optical adhesive 61 was dispensed on the surface, and then a clean piece of glass slide with an approximate area of 1 cm × 1 cm was placed on top of the drop, which spread to uniformly fill the gap between the glass slide and the gold surface. This process was repeated with additional pieces of glass, leaving lateral gaps of approximately 2−3 mm between the pieces. Finally, the optical adhesive was cured by illumination with a UV lamp for 3 h (UVP, model UVLS-28, 8 W) and further on the glass slide (with a gold layer adhered to it) and was mechanically cleaved from the wafer. As the exposed gold surface was in contact with the Si/SiO_2 surface, its roughness (RMS = 0.6 nm, measured by AFM) is smaller than that typically achieved by standard thermal metallization. We also measured a data set using substrates produced by standard metallization. Those substrates were prepared by thermal evaporation of a 10 nm Ti/10 nm Pd adhesion layer on a clean Si 100 surface, followed by a topmost 200 nm Au layer.

Layer-by-Layer Self-Assembly. Multilayer films were prepared on freshly cleaved TS gold substrates. We first conferred a negative surface charge to the substrate by depositing a layer of 3-mercapto-1-propanesulfonate (MPS) by immersion in a 10 mM MPS solution in 20 mM H_2SO_4 for 30 min. After rising with Milli-Q water, we deposited the first layer of PAH by immersion for 15 min in a 1 mg/mL solution, rinsed the sample, and dried it with nitrogen. The procedure was then repeated to deposit subsequent PAA (1 mg/mL) and PAH layers until the deposition of the desired number of layers was achieved. The pH of the PAH and PAA deposition solutions was 8 and 4, respectively, except for the experiments described at the end of the Supporting Information, where both solutions had pH 7.

Atomic Force Microscopy (AFM). AFM imaging was performed in air using an Agilent 5500 scanning probe microscope (Agilent Technologies) isolated from vibrations, air turbulence, and acoustic noise. Images were acquired using an insulating Si tip PointProbe Plus PPP-CONT (radius of <10 nm, force constant of 0.2 $N{\cdot}m^{-1}$, resonance frequency of 13 kHz) in contact mode. The surface topography of the layer-by-layer (LbL) films was imaged with AFM using near zero force (typically −0.5 V) and a scan rate of 1 line/s. The 1D statistical functions (height distribution plots) were calculated after removing part of the multilayer film by mechanical etching with the AFM tip. Briefly, a selected region (1 μm × 1 μm) was scanned repeatedly using a set point voltage of 9.3 V with a scan rate of 5 lines/s. Thereafter, the set point voltage was lowered back to −0.5 V and the scan area was set to 5 μm × 5 μm to get images containing film-stripped regions. In further analysis, images were properly flattened and cropped to expose equal areas of the substrate and the film. Finally, selected regions were analyzed with Gwyddion V2.49 in order to obtain 1D statistical functions. All AFM measurements were carried out over the same samples used for EGaIn measurements.

EGaIn Measurements. Our EGaIn setup was built following previous works from Whitesides[10,12] and Weiss[36] groups, with some differences as described next (see the Supporting Information for further details). The EGaIn setup was mounted on a commercial contact-angle setup to use its mechanical stage and camera (Figure S1a,b). We loaded the EGaIn in a Hamilton syringe (705RN, volume 50 μL) equipped with a blunt 22 gauge needle (point style 3, PN 7780-04) with an outer diameter of 0.7 mm. The EGaIn tip was produced as follows (see Figure S1c): we first formed an $EGaIn/Ga_2O_3$ drop at the tip of the needle and then slowly pulled the syringe upward to produce a conical tip. The $EGaIn/Ga_2O_3$ tip was then put in contact with a freshly cleaved gold TS surface. The average contact diameters and areas in all experiments reported were (0.13 ± 0.04) mm and (0.014 ± 0.009) mm^2, respectively.

https://doi.org/10.1021/acs.jpcc.2c02175
J. Phys. Chem. C 2022, 126, 9956−9964

Table 1. Summary of EGaIn Measurements for $(PAH/PAA)_m$ Films Deposited on TS Gold Substrates

M	film	$\langle \ln(\lvert Z\rvert_{lf} \cdot A)\rangle$	valid measurements	short circuits	noisy/irreproducible measurements
0.5	PAH	5.5 ± 1.7	11	11	8
1	PAH/PAA	8.4 ± 1.4	13	16	5
1.5	(PAH/PAA)PAH	8.5 ± 1.7	16	2	3
2	$(PAH/PAA)_2$	15.2 ± 2.7	27	1	0
2.5	$(PAH/PAA)_2PAH$	12.3 ± 1.9	14	0	4
3	$(PAH/PAA)_3$	17.6 ± 1.5	8	0	3

The impedance measurement setup consisted of a frequency response analyzer (FRA) outputted to the EGaIn/Ga_2O_3 top contact and a current amplifier (CA) (either a commercial Keithley 428 or a homemade transimpedance amplifier) connected between the sample and the FRA input. The FRA (Nf Electronic Instruments S5720c) had a bandwidth of 0.1 mHz to 100 kHz, although measurements were limited to the 0.01 Hz to 100 kHz range. In order to reduce electrical noise, we minimized the length of the unshielded cables and placed the setup (i.e., the contact angle meter) in a home-built Faraday cage. The FRA was connected to a computer via a GPIB (IEEE 488) interface and controlled by a custom written software. In a typical experiment, for each junction, we measured four impedance spectra using different CA scales (typically, the 10^4, 10^5, 10^6, and 10^7 V/A scales of the homemade CA) by scanning the signal frequency from 0.01−1 Hz to 100 kHz, taking 10 samples per decade.

We measured 11−30 junctions per sample (Table 1) in different sectors of the surface to map possible macroscopic heterogeneities. For each junction, a new EGaIn tip was generated, following the procedure described in the Supporting Information. Data from short-circuit and unstable junctions were discarded. Short circuits are recognizable in impedance measurements by having a constant zero phase, as well as a low ($<10^4$ Ω) resistance. Unstable junctions produced different impedance spectra in subsequent measurements. Note that while the data analysis in DC EGaIn measurements of alkanethiols SAMs usually employs all data,[11] this is unpractical for AC measurements in LbL films because of the need to record full impedance spectra for each junction and because samples with small number of layers (m < 1.5) exhibit a very large fraction of short circuits.

RESULTS AND DISCUSSION

We deposited layer-by-layer films of poly(allylamine) (PAH) and poly(acrylic acid) (PAA)[33,34] on flat template-stripped gold substrates[35] and measured their electrical properties using the EGaIn method developed by Whitesides and co-workers.[12] This method employs a liquid eutectic gallium/indium alloy (EGaIn) to make a conformal electrical top contact on the film, while the bottom contact is the gold substrate on which the film was deposited. Following first report of the EGaIn method,[12] different self-assembled systems, such as alkanethiol SAMs,[9,12,25] oligophenyleneimine SAMs,[37] redox-active benzo-tetrathiafulvalene SAMs,[38] photosystem I,[15] and others, were studied with DC or AC potentiostatic measurements. In the DC experiment, the steady-state currents are recorded as a function of the applied potential, which is typically scanned between −1 V and +1 V. Each measurement yields a I/V trace, and typically, many of such traces are measured per junction. The DC experiment not only allows to accurately determine the current density in the low-bias regime but also provides information about the density of states of the molecules between the two electrodes.[38] On the other hand, in the AC experiment, a low amplitude (typically ≤100 mV) sine wave function centered at 0 V with varying frequency (f) is applied to the sample and both the impedance modulus and the phase between I and V are recorded to obtain the complex impedance spectra of the system, $Z(f)$. This methodology allows us to discriminate between contributions to the total junction impedance at different time scales. In this way, phenomena such as dielectric effects and ionic conductance can be studied quantitatively.[39−41] In the case of alkanethiol SAMs measured with EGaIn top contacts, Nijhuis and co-workers[9] showed that both DC measurements and the low-frequency impedance measured by AC yield similar β values. The polyelectrolyte multilayer films under study contain electrically charged polymeric moieties ($-NH_3^+$ and $-COO^-$) and ions (Na^+ and Cl^-), so we used the AC technique in order to rule out transport mechanisms different from electron tunneling.

Figure 1a and Figure 1b show the impedance spectra of PAH/PAA films with different number of bilayers, m. Films with integer m are terminated in PAA, i.e., m = 2 and 2.5 indicate $(PAH/PAA)_2$ and $(PAH/PAA)_2PAH$, respectively. For all films, there is a threshold frequency below which the impedance modulus, |Z|, reaches a plateau (Figure 1a) and its phase becomes zero (Figure 1b). In those conditions (low frequency) the junction presents a purely resistive (ohmic) behavior. The amplitude of the sine wave was selected to be 100 mV (peak to peak) in order to reduce noise, but we observed no significant differences with impedance spectra recorded with amplitudes in the 10−100 mV range. We thus concluded that the impedance response of the system is in the linear regime (Figure S2).

Figure 1c shows a plot of the average $\ln(\lvert Z\rvert_{lf} \cdot A)$ vs the average film thickness measured by atomic force microscopy (AFM), h, where A is the contact area and $\lvert Z\rvert_{lf}$ is the impedance modulus at low frequencies (|Z| at the plateau). The data in Figure 1c include all measurements for each film except short circuits and unstable junctions. Figure 2 shows the histograms for the $\langle \ln(\lvert Z\rvert_{lf} \cdot A)\rangle$ values obtained in valid measurements. Table 1 summarizes the average $\langle \ln(\lvert Z\rvert_{lf} \cdot A)\rangle$ values and the numbers of valid measurements, short-circuits, and unstable junctions for all samples. Note that the number of short-circuits decreases as the number of layers increases, which is expected considering that the number of defects resulting from the intrinsic roughness of multilayer thin films[42] should decrease with increasing film thickness. We tested if the data obtained for each sample follow a normal distribution using the Shapiro−Wilk test and found that $\ln(\lvert Z\rvert_{lf} \cdot A)$ is normally distributed (except for m = 2, which shows a bimodal distribution; see Figure 2), while $\lvert Z\rvert_{lf}$ is not normally distributed; see Supporting Information. The same result was previously observed for alkanethiol SAMs.[4] As expected from

https://doi.org/10.1021/acs.jpcc.2c02175
J. Phys. Chem. C 2022, 126, 9956−9964

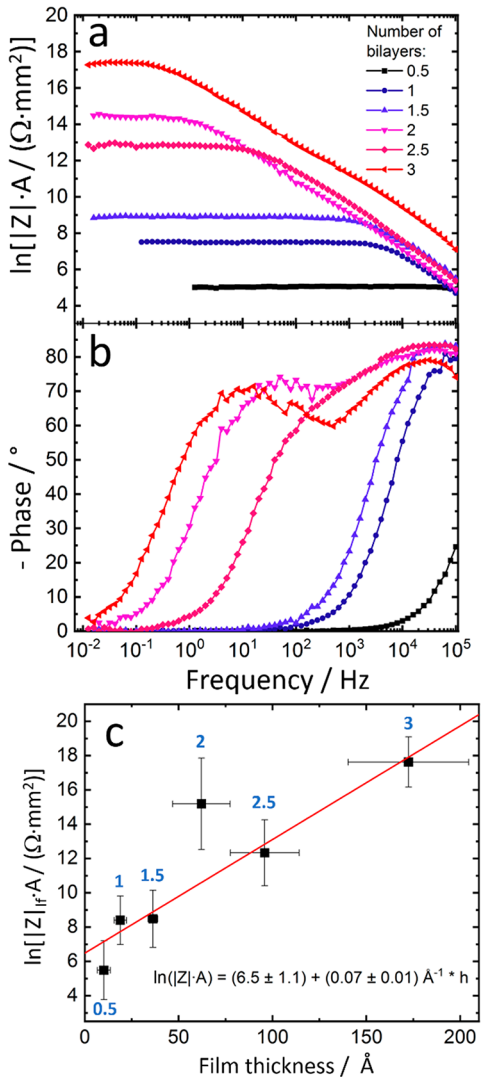

Figure 1. Impedance modulus (multiplied by the geometric area A) (a) and phase (b) measured for PAH/PAA multilayers. (c) Average $\ln(|Z|_{lf}\cdot A)$ vs film thickness for the results in part b (the number of bilayers is indicated next to each symbol). The symbols and error bars indicate the mean and one standard deviation, respectively.

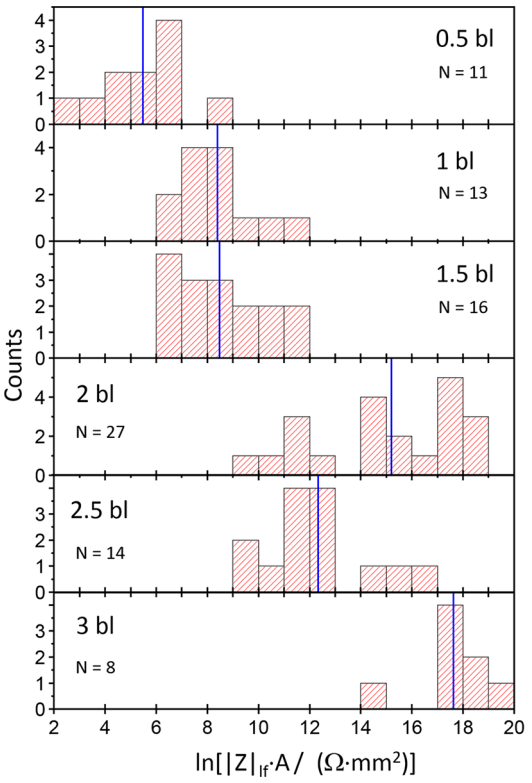

Figure 2. Histograms of $\ln(|Z|_{lf}\cdot A)$, where $|Z|_{lf}$ is the impedance modulus in the low-frequency region, for PAH/PAA films with different number of layers. N is the number of measurements for each sample. Vertical blue lines show the average values.

normally distributed data, the mean value of the distribution, $\langle \ln(|Z|_{lf}\cdot A)\rangle$, is very close to its median (Figure S11).

Figure 1c, Figure 2, and Table 1 show that the average $\ln(|Z|_{lf}\cdot A)$ systematically increases with the number of bilayers except for $m = 2$, which was more resistive than $m = 2.5$ (the reproducibility of this result was confirmed on additional samples of these films). This result may have an origin in the well-known oscillations of the properties and composition of polyelectrolyte multilayers with the number of adsorbed layers.[43,44]

We conclude that electron tunneling and not ionic conductivity (which may be expected in polyelectrolyte films) is the transport mechanism below the threshold frequency because (i) the observed low-frequency impedance is purely ohmic (phase equal to zero), while a nonzero phase is expected for ion transport because of the double-layer capacitance of the electrodes (Figure S3),[40,45] (ii) $|Z|_{lf}$ increases exponentially with film thickness (Figure 1c) as expected for electron tunneling (ion transport would produce a linear increase), (iii) $|Z|_{lf}$ is temperature insensitive (Figure S4), as expected for electron tunneling,[17] while ionic conductivity should increase with temperature,[40,45,46] and (iv) the resistances expected from ionic conductivities reported in the literature[40,45] are much larger than those in Figure 1 (Table S2). Also note that the impedance spectra in Figure 1a are strikingly similar to those measured for electron tunneling through SAMs of alkanethiols of different lengths.[9,37] In those studies, the impedance spectroscopy data also showed a capacitive behavior at high frequency and a resistive behavior at low frequency.

The simplified Simmons model for electron tunneling[16] predicts $|Z|_{lf}\cdot A \sim \exp(\beta h)$, where the β is the tunneling decay coefficient. Applying the model to our data (best linear fitting in Figure 1c) yields $\beta^{app} = (0.07 \pm 0.01)$ Å^{-1}, where "app" stands for apparent because (as we show below) this value does not correspond to the real β of the junction. Typically, $\beta = 0.79-0.83$ Å^{-1} for SAMs of unconjugated alkanethiols,[11] and $\beta \sim 0.1-0.3$ Å^{-1} for SAMs of molecules with conjugated double bonds.[17,37,47] Considering that our PAH/PAA films do not contain extended π orbitals, the value of $\beta^{app} = (0.07 \pm 0.01)$ Å^{-1} (which corresponds to very long-range tunneling) seems unrealistically low, even considering the presence of polarizable species like $-NH_2$ and $-COOH$ groups which may contribute to a lowering in the electron tunneling barrier, as discussed in the Introduction. The measurement of film thickness does not introduce large errors; the values of h determined with AFM are within 10% of those independently measured by ellipsometry (Figure S6). The roughness of the substrate and the sample-to-sample reproducibility also do not seem to be critical: the values of $\langle \ln(|Z|_{lf}\cdot A)\rangle$ reported in Figure 1c are not significantly different from those measured for LbL

https://doi.org/10.1021/acs.jpcc.2c02175
J. Phys. Chem. C 2022, 126, 9956−9964

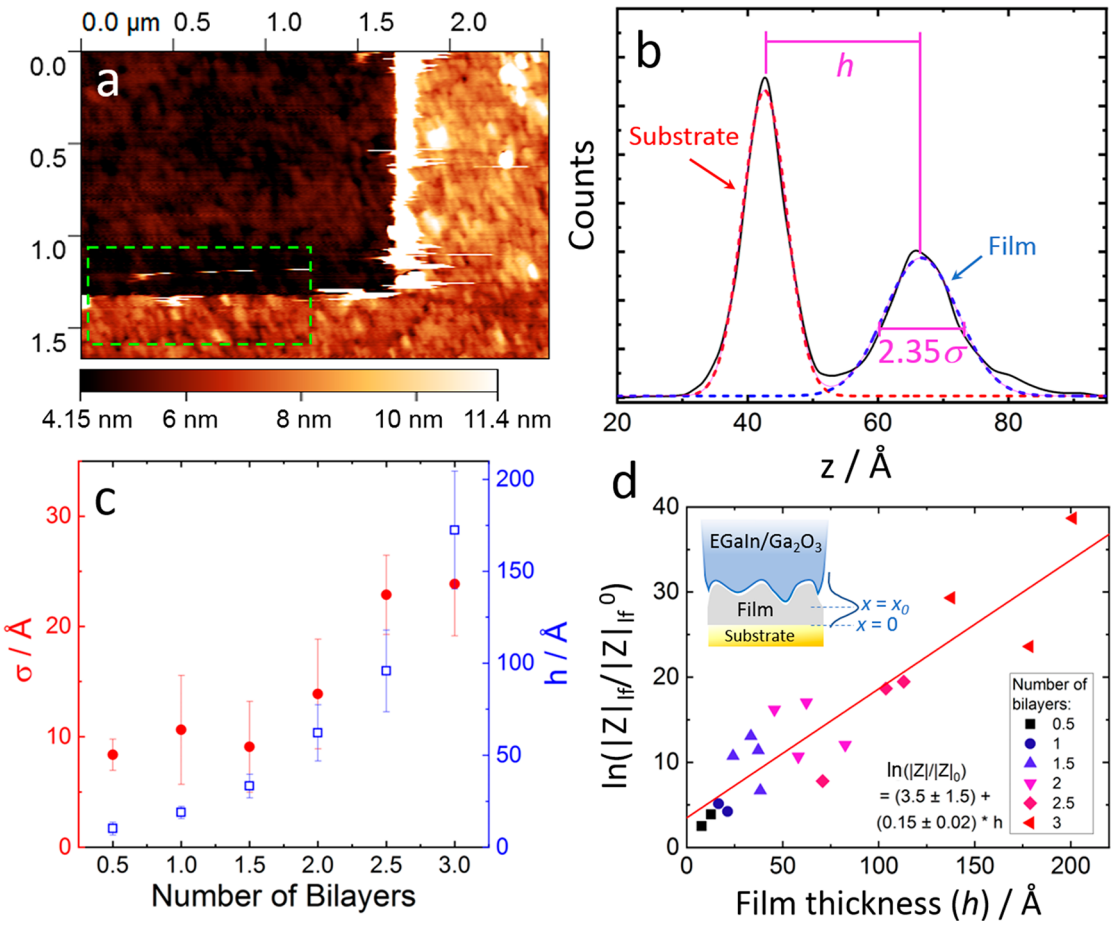

Figure 3. (a) AFM topography image of a 1.5 bilayer PAH/PAA film. In the upper-left region of the image, the film was mechanically removed using the AFM tip. (b) Histogram of the height distribution within the green box shown in panel a. Red and blue dashed lines represent the best fit Gaussian functions resulting from fitting the histogram with a sum of two Gaussians. The film thickness (h) and its standard deviation (σ) were determined as indicated. (c) Average of h (solid circles) and σ (open squares) for the samples used for EGaIn measurements vs number of bilayers. (d) $\ln(|Z|_{lf}/|Z|^0_{lf})$ vs h calculated with the model for tunneling through inhomogeneous films, eqs 4 and 5. Each point corresponds to a different AFM image.

films prepared on standard thermally evaporated gold substrates (i.e., Si 100 coated by thermal evaporation with 10 nm Ti, 10 nm Pd, 200 nm Au); see Figure S10. Moreover, we found $\beta^{app} = (0.14 \pm 0.04)$ Å^{-1} for multilayers deposited at pH = 7, where the thickness per bilayer is smaller than for that of the films measured in Figure 1 (deposited using pH = 8 for PAH and 4 for PAA); see Figure S7. These results indicate that the smaller-than-expected β^{app} is a robust result for PAH/PAA films.

The homogeneity of film thickness is a major difference between alkanethiol SAMs and polyelectrolyte multilayers. The thickness of SAMs is given by the molecular length of the thiol, so it exhibits very small fluctuations. The thickness of polyelectrolyte multilayers has strong fluctuations that arise from different polymer conformations. To characterize the height distribution of our films, we performed AFM experiments by mechanically removing part of the films using the AFM tip; see example in Figure 3a. Figure 3b shows a histogram of the height distribution in the region delimited with a green rectangle in Figure 3a. The histogram has two peaks, corresponding to the substrate (left peak) and the film (right peak). The flat template-stripped gold substrates used in this work minimize the roughness of the substrate,[35] resulting in peak widths for the substrate that were consistently smaller (~60% smaller on average) than those of the film (see Figure 3b). We fitted the peaks in the histogram in Figure 3b with the sum of two Gaussian functions and obtained the average film thickness, h, and its standard deviation, σ, as shown in Figure 3b. We conducted this AFM experiment (at least in duplicate) for the same films used in the EGaIn measurements and report h and σ in Figure 3c (see Table S2 for all fitting parameters). Figure 3c reveals that both h and σ increase monotonically with the number of bilayers and that the relative thickness fluctuations are large (σ/h = 0.14–0.82).

To test our hypothesis that $\beta^{app} \ll \beta$ because of thickness fluctuations, let us consider electron tunneling through a large-area junction presenting an approximately Gaussian distribution of local thicknesses (in agreement with the AFM experiments in Figure 3b). Assuming a flat substrate located at $x = 0$ and that the EGaIn/Ga_2O_3 conformally adapts to the surface of the film (see inset in Figure 3d), then the total current density (j) is given by

$$j = j_0 \int_0^\infty P(x) \exp(-\beta x)\, dx \qquad (2)$$

where j_0 is the injection tunnel current density (ideal current for $h = 0$) and

https://doi.org/10.1021/acs.jpcc.2c02175
J. Phys. Chem. C 2022, 126, 9956−9964

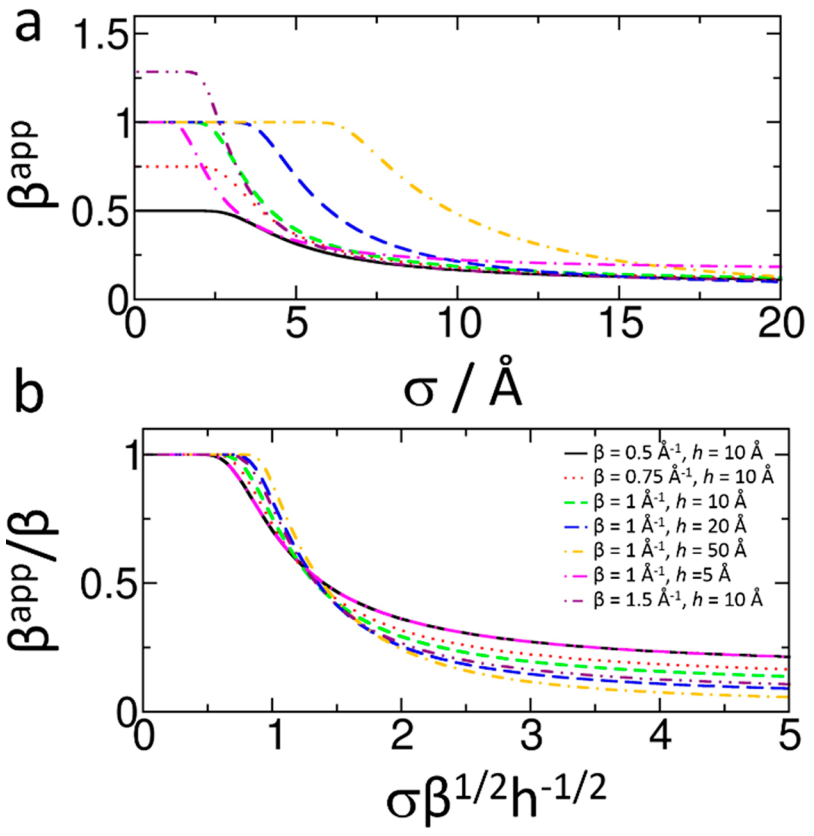

Figure 4. (a) β^{app} vs σ (standard deviation of film thickness) for different values of β and h calculated with eqs 4−6. (b) β^{app}/β vs the dimensionless parameter $\sigma\beta^{1/2}h^{-1/2}$.

$$P(x) = \frac{1}{A}\exp\left(-\frac{1}{2}\frac{(x - x_0)^2}{\sigma^2}\right) \tag{3}$$

is a Gaussian distribution, in which A is a normalization constant that ensures $\int_0^\infty P(x)\,dx = 1$. The lower limit of the integral is zero because the substrate is present at $x = 0$ (see inset in Figure 3d). Equation 2 has the following analytical solution,

$$j = j_0 \frac{\exp\left(\frac{(\beta\sigma)^2}{2} - \beta x_0\right)\mathrm{erfc}\left(\sqrt{\frac{1}{2}}\left(\beta\sigma - \frac{x_0}{\sigma}\right)\right)}{\mathrm{erfc}\left(-\sqrt{\frac{1}{2}}\frac{x_0}{\sigma}\right)} \tag{4}$$

where erfc is the complementary error function. The average film thickness, h, is

$$h = \int_0^\infty P(x)x\,dx = x_0 + \sigma\frac{\exp\left(-\frac{1}{2}\left(\frac{x_0}{\sigma}\right)^2\right)}{\sqrt{\frac{\pi}{2}}\left(\mathrm{erfc}\left(-\sqrt{\frac{1}{2}}\frac{x_0}{\sigma}\right)\right)} \tag{5}$$

Note that the average film thickness is slightly larger than the mean of the Gaussian, x_0, because of the presence of the substrate (see Figure S9), e.g., $x_0/h = 0.97$ for a typical value of $\sigma/h = 0.5$.

We used eqs 4 and 5 to obtain j from the h and σ values determined in each AFM experiment (Table S2), using $\beta = 1$ Å^{-1}. We then calculated $|Z|/|Z_0| = |j_0|/|j|$ and plotted $\ln(|Z|/|Z_0|)$ vs h in Figure 3d. The slope of the plot results in $\beta^{app} = (0.15 \pm 0.02)$ Å^{-1}. This value is much smaller than the value of β used in the calculations (1 Å^{-1}), and thus it demonstrates that thickness fluctuations result in artificially low tunneling decay coefficients. Film thickness fluctuations produce $\beta^{app} < \beta$ because the electron tunneling current is dominated by the thinnest regions of the film. The discrepancy between the predicted β^{app} [(0.15 ± 0.02) Å^{-1}] and that measured by EGaIn [β = (0.07 ± 0.01) Å^{-1}] probably resides in the assumption that the thickness has a perfect Gaussian distribution. The terms with small x contribute the most in the integral of eq 2; however these terms are in the tail of the Gaussian; thus small deviations from a perfect Gaussian functionality (which are apparent in Figure 3b) introduce large errors. On the other hand, the value of β used in the calculation is not a source of error since it has a very minor impact on β^{app}: using $\beta = 0.5$ Å^{-1} does not affect β^{app} within the uncertainty of our measurements. This important result reveals a regime where the apparent tunneling coefficient is exclusively dominated by thickness fluctuations, and consequently, it is impossible to determine β.

Mathematically, β^{app} depends on x_0 (which is very close to h), β, and σ. Because β^{app} depends on x_0, $\ln(|Z|/|Z_0|)$ is not guaranteed to be a linear function of h (the scattering of the experimental data in Figure 3d prevents checking for potential deviations from linearity). Therefore, it is useful to consider an operational definition of β^{app}:

$$\beta^{app} = \left(\frac{\partial \log(|Z|/|Z_0|)}{\partial h}\right)_{\sigma,\beta} \tag{6}$$

Figure 4a shows β^{app} vs σ for different values of h and β. Note that for $\sigma > h$, β^{app} becomes independent of β, as discussed above. Figure 4b show a plot of β^{app}/β vs the

https://doi.org/10.1021/acs.jpcc.2c02175
J. Phys. Chem. C 2022, 126, 9956−9964

dimensionless variable $\sigma\beta^{1/2}h^{-1/2}$, which shifts all curves so they intercept at $\beta^{app}/\beta = 0.5$ and $\sigma\beta^{1/2}h^{-1/2} = \sqrt{2}$. For films with $\sigma\beta^{1/2}h^{-1/2} \gtrsim 0.8$, thickness fluctuations lead to $\beta^{app} < \beta$. That is the case of our films, which have $1.0 < \beta^{1/2}\sigma h^{-1/2} < 3.4$ (using $\beta = 1$ Å^{-1}). For a typical alkanethiol SAM ($\beta = 0.75$ Å^{-1}, $h = 10$ Å),[11] $\beta^{app} < \beta$ requires $\sigma > 2.9$ Å (i.e., 2.3 C−C bonds). It is unlikely that such large fluctuations occur for close-packed defect-free SAMs; however, β values in alkanethiol SAMs are known to decrease with increasing content of defects,[4,18,30] in line with the predictions of our model.

CONCLUSIONS

In summary, we identified a tunneling charge-transfer mechanism in large-area Au/multilayer film/Ga_2O_3/EGaIn junctions using impedance spectroscopy. Analyzing the low-frequency resistance of the films with the Simmons model resulted in an unusually low value of the tunneling decay constant, $\beta = 0.07 \pm 0.01$ Å^{-1}. AFM measurements revealed that the films have nearly Gaussian thickness distributions. We input these distributions into a theoretical model that considers electron tunneling through a barrier of inhomogeneous thickness and obtained apparent β values that were always smaller than the intrinsic β of the material. These results indicate that thickness fluctuations are likely responsible for the smaller-than-expected values of β obtained for LbL multilayers. While this effect is unlikely to strongly affect measurements in closed-packed defect-free SAMs, it will be relevant for SAMs with defects (e.g., resulting from imperfect packing at grain boundaries[4,18]). Moreover, the effect will be critical for highly disordered materials, such as the polyelectrolyte multilayers studied here. In those systems, thickness fluctuations may completely prevent the determination of the tunneling parameters.

ASSOCIATED CONTENT

Supporting Information

The Supporting Information is available free of charge at https://pubs.acs.org/doi/10.1021/acs.jpcc.2c02175.

Additional experimental methods, detailed discussion of the charge transport mechanism across the junctions, alternative determination of film thickness with ellipsometry, fitting parameters for AFM experiments, summary of EGaIn measurements for films deposited at pH 7 and plots of Gaussian functions and average film thickness, comparison of data sets obtained for LbL films on TS and thermally evaporated gold surfaces, and statistical distribution of impedance measurements (PDF)

AUTHOR INFORMATION

Corresponding Authors

Santiago E. Herrera − *Facultad de Ciencias Exactas y Naturales, Departamento de Química Inorgánica Analítica y Química Física, Universidad de Buenos Aires, Ciudad Autónoma de Buenos Aires C1428EGA, Argentina; Facultad de Ciencias Exactas y Naturales, Instituto de Química de los Materiales, Ambiente y Energía (INQUIMAE), CONICET—Universidad de Buenos Aires, Ciudad Autónoma de Buenos Aires C1428EGA, Argentina;* orcid.org/0000-0002-8327-3914; Email: sherrera@qi.fcen.uba.ar

Mario Tagliazucchi − *Facultad de Ciencias Exactas y Naturales, Departamento de Química Inorgánica Analítica y Química Física, Universidad de Buenos Aires, Ciudad Autónoma de Buenos Aires C1428EGA, Argentina; Facultad de Ciencias Exactas y Naturales, Instituto de Química de los Materiales, Ambiente y Energía (INQUIMAE), CONICET—Universidad de Buenos Aires, Ciudad Autónoma de Buenos Aires C1428EGA, Argentina;* orcid.org/0000-0003-4755-955X; Email: mario@qi.fcen.uba.ar

Authors

Liliana Maldonado − *Facultad de Ciencias Exactas y Naturales, Departamento de Química Inorgánica Analítica y Química Física, Universidad de Buenos Aires, Ciudad Autónoma de Buenos Aires C1428EGA, Argentina; Facultad de Ciencias Exactas y Naturales, Instituto de Química de los Materiales, Ambiente y Energía (INQUIMAE), CONICET—Universidad de Buenos Aires, Ciudad Autónoma de Buenos Aires C1428EGA, Argentina*

Federico J. Williams − *Facultad de Ciencias Exactas y Naturales, Departamento de Química Inorgánica Analítica y Química Física, Universidad de Buenos Aires, Ciudad Autónoma de Buenos Aires C1428EGA, Argentina; Facultad de Ciencias Exactas y Naturales, Instituto de Química de los Materiales, Ambiente y Energía (INQUIMAE), CONICET—Universidad de Buenos Aires, Ciudad Autónoma de Buenos Aires C1428EGA, Argentina;* orcid.org/0000-0002-6194-2734

Complete contact information is available at: https://pubs.acs.org/10.1021/acs.jpcc.2c02175

Notes

The authors declare no competing financial interest.

ACKNOWLEDGMENTS

S.E.H., F.J.W., and M.T. are Fellows of CONICET. We acknowledge financial support from CONICET (Grant PIP 11220200102008CO) and Agencia Nacional de Promoción Científica y Tecnológica (Grants PICT 4649-2018, PICT 1520-2019, and PICT 0035-2020).

REFERENCES

(1) Kim, T.-W.; Wang, G.; Lee, H.; Lee, T. Statistical Analysis of Electronic Properties of Alkanethiols in Metal−Molecule−Metal Junctions. *Nanotechnology* **2007**, *18* (31), 315204.

(2) Wang, G.; Kim, Y.; Choe, M.; Kim, T.; Lee, T. A New Approach for Molecular Electronic Junctions with a Multilayer Graphene Electrode. *Adv. Mater.* **2011**, *23* (6), 755−760.

(3) Slowinski, K.; Fong, H. K.; Majda, M. Mercury− Mercury Tunneling Junctions. 1. Electron Tunneling across Symmetric and Asymmetric Alkanethiolate Bilayers. *J. Am. Chem. Soc.* **1999**, *121* (31), 7257−7261.

(4) Weiss, E. A.; Chiechi, R. C.; Kaufman, G. K.; Kriebel, J. K.; Li, Z.; Duati, M.; Rampi, M. A.; Whitesides, G. M. Influence of Defects on the Electrical Characteristics of Mercury-Drop Junctions: Self-Assembled Monolayers of n-Alkanethiolates on Rough and Smooth Silver. *J. Am. Chem. Soc.* **2007**, *129* (14), 4336−4349.

(5) Milani, F.; Grave, C.; Ferri, V.; Samorì, P.; Rampi, M. A. Ultrathin Π-conjugated Polymer Films for Simple Fabrication of Large-area Molecular Junctions. *ChemPhysChem* **2007**, *8* (4), 515−518.

(6) Cui, X.; Zarate, X.; Tomfohr, J.; Sankey, O. F.; Primak, A.; Moore, A.; Moore, T.; Gust, D.; Harris, G.; Lindsay, S. M. Making

Electrical Contacts to Molecular Monolayers. *Nanotechnology* **2002**, *13* (1), 5.
(7) Song, H.; Lee, H.; Lee, T. Intermolecular Chain-to-Chain Tunneling in Metal− Alkanethiol− Metal Junctions. *J. Am. Chem. Soc.* **2007**, *129* (13), 3806−3807.
(8) Nijhuis, C. A.; Reus, W. F.; Barber, J. R.; Whitesides, G. M. Comparison of SAM-Based Junctions with Ga2O3/EGaIn Top Electrodes to Other Large-Area Tunneling Junctions. *J. Phys. Chem. C* **2012**, *116* (26), 14139−14150.
(9) Sangeeth, C. S.; Wan, A.; Nijhuis, C. A. Equivalent Circuits of a Self-Assembled Monolayer-Based Tunnel Junction Determined by Impedance Spectroscopy. *J. Am. Chem. Soc.* **2014**, *136* (31), 11134−11144.
(10) Weiss, E. A.; Porter, V. J.; Chiechi, R. C.; Geyer, S. M.; Bell, D. C.; Bawendi, M. G.; Whitesides, G. M. The Use of Size-Selective Excitation To Study Photocurrent through Junctions Containing Single-Size and Multi-Size Arrays of Colloidal CdSe Quantum Dots. *J. Am. Chem. Soc.* **2008**, *130* (1), 83−92.
(11) Simeone, F. C.; Yoon, H. J.; Thuo, M. M.; Barber, J. R.; Smith, B.; Whitesides, G. M. Defining the Value of Injection Current and Effective Electrical Contact Area for EGaIn-Based Molecular Tunneling Junctions. *J. Am. Chem. Soc.* **2013**, *135* (48), 18131−18144.
(12) Chiechi, R. C.; Weiss, E. A.; Dickey, M. D.; Whitesides, G. M. Eutectic Gallium−Indium (EGaIn): A Moldable Liquid Metal for Electrical Characterization of Self-Assembled Monolayers. *Angew. Chem. Int. Ed* **2008**, *47* (1), 142−144.
(13) Liu, Y.; Qiu, X.; Soni, S.; Chiechi, R. C. Charge Transport through Molecular Ensembles: Recent Progress in Molecular Electronics. *Chem. Phys. Rev.* **2021**, *2* (2), 021303.
(14) Kumar, K. S.; Pasula, R. R.; Lim, S.; Nijhuis, C. A. Long-Range Tunneling Processes across Ferritin-Based Junctions. *Adv. Mater.* **2016**, *28* (9), 1824−1830.
(15) Castañeda Ocampo, O. E.; Gordiichuk, P.; Catarci, S.; Gautier, D. A.; Herrmann, A.; Chiechi, R. C. Mechanism of Orientation-Dependent Asymmetric Charge Transport in Tunneling Junctions Comprising Photosystem I. *J. Am. Chem. Soc.* **2015**, *137* (26), 8419−8427.
(16) Simmons, J. G. Generalized Formula for the Electric Tunnel Effect between Similar Electrodes Separated by a Thin Insulating Film. *J. Appl. Phys.* **1963**, *34* (6), 1793−1803.
(17) Khoo, K. H.; Chen, Y.; Li, S.; Quek, S. Y. Length Dependence of Electron Transport through Molecular Wires−a First Principles Perspective. *Phys. Chem. Chem. Phys.* **2015**, *17* (1), 77−96.
(18) Yuan, L.; Jiang, L.; Zhang, B.; Nijhuis, C. A. Dependency of the Tunneling Decay Coefficient in Molecular Tunneling Junctions on the Topography of the Bottom Electrodes. *Angew. Chem.* **2014**, *126* (13), 3445−3449.
(19) Vilan, A.; Aswal, D.; Cahen, D. Large-Area, Ensemble Molecular Electronics: Motivation and Challenges. *Chem. Rev.* **2017**, *117* (5), 4248−4286.
(20) Akkerman, H. B.; de Boer, B. Electrical Conduction through Single Molecules and Self-Assembled Monolayers. *J. Phys.: Condens. Matter* **2008**, *20* (1), 013001.
(21) Venkataraman, L.; Klare, J. E.; Tam, I. W.; Nuckolls, C.; Hybertsen, M. S.; Steigerwald, M. L. Single-Molecule Circuits with Well-Defined Molecular Conductance. *Nano Lett.* **2006**, *6* (3), 458−462.
(22) Li, X.; He, J.; Hihath, J.; Xu, B.; Lindsay, S. M.; Tao, N. Conductance of Single Alkanedithiols: Conduction Mechanism and Effect of Molecule− Electrode Contacts. *J. Am. Chem. Soc.* **2006**, *128* (6), 2135−2141.
(23) Gu, M.-W.; Peng, H. H.; Chen, I-W. P.; Chen, C.-h. Tuning Surface d Bands with Bimetallic Electrodes to Facilitate Electron Transport across Molecular Junctions. *Nat. Mater.* **2021**, *20* (5), 658−664.
(24) Peng, L.-L.; Huang, B.; Zou, Q.; Hong, Z.-W.; Zheng, J.-F.; Shao, Y.; Niu, Z.-J.; Zhou, X.-S.; Xie, H.-J.; Chen, W. Low Tunneling Decay of Iodine-Terminated Alkane Single-Molecule Junctions. *Nanoscale Res. Lett.* **2018**, *13* (1), 121.
(25) Chen, X.; Kretz, B.; Adoah, F.; Nickle, C.; Chi, X.; Yu, X.; Del Barco, E.; Thompson, D.; Egger, D. A.; Nijhuis, C. A. A Single Atom Change Turns Insulating Saturated Wires into Molecular Conductors. *Nat. Commun.* **2021**, *12* (1), 3432.
(26) Sangtarash, S.; Vezzoli, A.; Sadeghi, H.; Ferri, N.; O'Brien, H. M.; Grace, I.; Bouffier, L.; Higgins, S. J.; Nichols, R. J.; Lambert, C. J. Gateway State-Mediated, Long-Range Tunnelling in Molecular Wires. *Nanoscale* **2018**, *10* (6), 3060−3067.
(27) Amdursky, N.; Marchak, D.; Sepunaru, L.; Pecht, I.; Sheves, M.; Cahen, D. Electronic Transport via Proteins. *Adv. Mater.* **2014**, *26* (42), 7142−7161.
(28) Zhang, Y.; Liu, C.; Balaeff, A.; Skourtis, S. S.; Beratan, D. N. Biological Charge Transfer via Flickering Resonance. *Proc. Natl. Acad. Sci.* **2014**, *111* (28), 10049−10054.
(29) Ha, T. Q.; Planje, I. J.; White, J. R.; Aragonès, A. C.; Díez-Pérez, I. Charge Transport at the Protein−Electrode Interface in the Emerging Field of BioMolecular Electronics. *Curr. Opin. Electrochem* **2021**, *28*, 100734.
(30) Jiang, L.; Sangeeth, C. S.; Yuan, L.; Thompson, D.; Nijhuis, C. A. One-Nanometer Thin Monolayers Remove the Deleterious Effect of Substrate Defects in Molecular Tunnel Junctions. *Nano Lett.* **2015**, *15* (10), 6643−6649.
(31) Levine, I.; Weber, S. M.; Feldman, Y.; Bendikov, T.; Cohen, H.; Cahen, D.; Vilan, A. Molecular Length, Monolayer Density, and Charge Transport: Lessons from Al−AlOx/Alkyl−Phosphonate/Hg Junctions. *Langmuir* **2012**, *28* (1), 404−415.
(32) Selzer, Y.; Salomon, A.; Cahen, D. The Importance of Chemical Bonding to the Contact for Tunneling through Alkyl Chains. *J. Phys. Chem. B* **2002**, *106* (40), 10432−10439.
(33) Decher, G. Fuzzy Nanoassemblies: Toward Layered Polymeric Multicomposites. *Science* **1997**, *277* (5330), 1232−1237.
(34) *Multilayer Thin Films: Sequential Assembly of Nanocomposite Materials*; Decher, G., Schlenoff, J. B., Eds.; Wiley: Weinheim, Germany, 2003.
(35) Weiss, E. A.; Kaufman, G. K.; Kriebel, J. K.; Li, Z.; Schalek, R.; Whitesides, G. M. Si/SiO2-Templated Formation of Ultraflat Metal Surfaces on Glass, Polymer, and Solder Supports: Their Use as Substrates for Self-Assembled Monolayers. *Langmuir* **2007**, *23* (19), 9686−9694.
(36) Lilly, G. D.; Whalley, A. C.; Grunder, S.; Valente, C.; Frederick, M. T.; Stoddart, J. F.; Weiss, E. A. Switchable Photoconductivity of Quantum Dot Films Using Cross-Linking Ligands with Light-Sensitive Structures. *J. Mater. Chem.* **2011**, *21* (31), 11492−11497.
(37) Sangeeth, C. S. S.; Demissie, A. T.; Yuan, L.; Wang, T.; Frisbie, C. D.; Nijhuis, C. A. Comparison of DC and AC Transport in 1.5−7.5 Nm Oligophenylene Imine Molecular Wires across Two Junction Platforms: Eutectic Ga−In versus Conducting Probe Atomic Force Microscope Junctions. *J. Am. Chem. Soc.* **2016**, *138* (23), 7305−7314.
(38) Han, Y.; Nickle, C.; Maglione, M. S.; Karuppannan, S. K.; Casado-Montenegro, J.; Qi, D.; Chen, X.; Tadich, A.; Cowie, B.; Mas-Torrent, M.; et al. Bias-Polarity-Dependent Direct and Inverted Marcus Charge Transport Affecting Rectification in a Redox-Active Molecular Junction. *Adv. Sci.* **2021**, *8* (14), 2100055.
(39) Chen, X.; Nijhuis, C. A. The Unusual Dielectric Response of Large Area Molecular Tunnel Junctions Probed with Impedance Spectroscopy. *Adv. Electron. Mater.* **2022**, *8* (2), 2100495.
(40) Durstock, M. F.; Rubner, M. F. Dielectric Properties of Polyelectrolyte Multilayers. *Langmuir* **2001**, *17* (25), 7865−7872.
(41) DeLongchamp, D. M.; Hammond, P. T. Fast Ion Conduction in Layer-by-Layer Polymer Films. *Chem. Mater.* **2003**, *15* (5), 1165−1173.
(42) Lobo, R. F. M.; Pereira-da-Silva, M. A.; Raposo, M.; Faria, R. M.; Oliveira, O. N. The Morphology of Layer-by-Layer Films of Polymer/Polyelectrolyte Studied by Atomic Force Microscopy. *Nanotechnology* **2003**, *14* (1), 101−108.
(43) Schönhoff, M.; Ball, V.; Bausch, A. R.; Dejugnat, C.; Delorme, N.; Glinel, K.; Klitzing, R. v; Steitz, R. Hydration and Internal

https://doi.org/10.1021/acs.jpcc.2c02175
J. Phys. Chem. C 2022, 126, 9956−9964

Properties of Polyelectrolyte Multilayers. *Colloids Surf. Physicochem. Eng. Asp* **2007**, *303* (1−2), 14−29.
(44) Tagliazucchi, M.; Calvo, E. J. Charge Transport in Redox Polyelectrolyte Multilayer Films: The Dramatic Effects of Outmost Layer and Solution Ionic Strength. *ChemPhysChem* **2010**, *11* (13), 2957−2968.
(45) Schönhoff, M.; Imre, A. W.; Bhide, A.; Cramer, C. Mechanisms of Ion Conduction in Polyelectrolyte Multilayers and Complexes. *Prog. Phys. Chem.* **2011**, *4*, 123−157.
(46) Imre, Á. W.; Schönhoff, M.; Cramer, C. A Conductivity Study and Calorimetric Analysis of Dried Poly (Sodium 4-Styrene Sulfonate)/Poly (Diallyldimethylammonium Chloride) Polyelectrolyte Complexes. *J. Chem. Phys.* **2008**, *128* (13), 134905.
(47) Ho Choi, S.; Kim, B.; Frisbie, C. D. Electrical Resistance of Long Conjugated Molecular Wires. *Science* **2008**, *320* (5882), 1482−1486.

https://doi.org/10.1021/acs.jpcc.2c02175
J. Phys. Chem. C 2022, 126, 9956−9964